Triethylamine borane thermal decomposition
for BN low pressure chemical vapour deposition

Pierre FENETAUD, Jérôme ROGER, Georges CHOLLON, Sylvain JACQUES*

LCTS UMR 5801, CNRS - University of Bordeaux, 3 allée de la Boétie, 33600 Pessac, France
*corresponding author

Abstract

Triethylamine borane (TEAB) complex was studied as a potential precursor for the chemical vapour deposition (CVD) of BN. In particular, its thermal decomposition with or without ammonia was characterised from thermodynamic and experimental points of view in the temperature ranges 400-2000 °C and 300-1300 °C respectively. NH_3 plays a role in the gas phase equilibrium by providing a nitriding source that promotes HCN formation at high temperatures. NH_3 is also a source of hydrogen for light hydrocarbons formation as it decomposes. It is thus possible to promote gaseous carbon species formation at high temperatures and limit carbon introduction into coatings by adding ammonia. A turbostratic BN coating could be obtained by CVD from a TEAB/NH_3/N_2 mixture and conditions chosen thanks to the gas phase decomposition study.

Keywords
Triethylamine borane; CVD; BN; FTIR; thermodynamics

1. Introduction

Hexagonal BN is a material that can be used in many applications thanks to its interesting properties [1]. Boron nitride is also used as an interphase in ceramic matrix composites (CMCs) for aircraft engines of the next generation. Indeed, the BN interphase gives to SiC-based CMCs a non-brittle mechanical behaviour and long lifetimes in oxidising/corrosive environments at high temperatures [2–4]. BN interphases are mainly produced by gas phase routes such as chemical vapour deposition (CVD) or, alternatively, chemical vapour infiltration. Boron trichloride combined with ammonia is classically used in industrial production. Yet, its corrosive nature, as well as its reaction by-products such as ammonium chloride (NH_4Cl), limit the use of this precursor [5,6].

Halogen-free organometallic precursors for BN deposition are an alternative [7,8]. In particular, triethylamine borane (TEAB) complex is a precursor that is liquid at room temperature, inexpensive and hardly aggressive. It offers a source of boron and nitrogen with 6 carbon atoms per molecule. The literature on the use of TEAB ((C_2H_5)$_3$N:BH_3) alone as a precursor in conventional CVD and plasma-enhanced CVD (PECVD) reports the formation of BNC coatings under a wide range of conditions [9–13]. The addition of ammonia is very effective in reducing the carbon content of the resulting coatings in both CVD [9,10,13–15] and PECVD [12,15–17]. However, only PECVD deposition has resulted in carbon-free compositions. Particularly in low pressure CVD (LPCVD), the works of Levy *et al.* [10] and Ramanuja [14] have identified two deposition regimes from TEAB, with or without ammonia addition. The addition of ammonia to the gas mixture limits the carbon contamination in the films deposited at

high temperature by forming HCN. This effect was also found with the tris(dimethylamino)borane/ammonia system [7,8].

The present study focused on the analysis of the thermal behaviour of TEAB, with or without NH_3, for the deposition of boron nitride by LPCVD, from a thermodynamic and experimental point of view. The aim was to provide insights into the growth mechanisms by which the composition of the coatings can be controlled. Fourier-transform infrared (FTIR) spectroscopy has been successfully used in previous CVD studies with other chemical systems [6,18]. This technique has been used here to detect, identify and follow the concentration of the species present in the gas phase at the reactor outlet. Finally, conditions were chosen based on the results of thermodynamic calculations and gas analyses to validate the feasibility of the desired material deposition. A coating was thereby synthesised by LPCVD and characterised.

2. Thermodynamic analysis of the decomposition of TEAB/NH_3 mixture

Thermodynamic equilibrium calculations based on Gibbs free energy minimization have been carried out in the H-B-C-N system based on the CALPHAD methodology (CALculation of PHAse Diagram) [19,20], using Thermo-Calc software [21]. They relied on a database drawn from various works and data in the literature [22–25]. The species considered in the calculations are listed in Table 1.

Gas					Solids
H1	N1	BH3	C2H5	C6H5	B
H2	N2	BH6N3	C2H6	C6H6	C (graphite)
B1	N3	B3H6N3	C3H3	C7H8	B4C
B2	B11C	C2N	C3H4	C8H8	BN
B12	BC2	C2N2	C3H6	C9H19	
C1	B2C	C4N2	C3H8	C10H8	
C2	NH3	CH3	C4H2	C12H10	
C3	N2H4	CH4	C4H4	HCN	
C4	BH2	C2H2	C4H6	H3C2N	
C5	B2H6	C2H4	C5H6		

Table 1 – Species considered in the thermodynamic calculations.

The initial mixtures examined consisted of the following:

(i)   TEAB/NH_3/N_2: 2.5 mol of TEAB, 40 mol of NH_3 and 212.5 mol of N_2.

(ii)   TEAB/N_2: 2.5 mol of TEAB and 252.5 mol of N_2.

The quantities of boron, carbon, hydrogen and nitrogen atoms introduced were therefore 2.5 moles, 15 moles, 165 moles and 467.5 moles reflecting the initial presence of NH_3 (i) and 2.5 moles, 15 moles, 45 moles and 507.5 moles in the absence of NH_3 (ii) respectively. Two sets of calculations were performed at a pressure of 55 mbar.

In the first set, all possible solid and gaseous species were included in the calculations to describe the equilibrium of the heterogeneous system. The results thus give the quantities present in each phase. The second set of calculations describes the evolution of the gas phase in the absence of condensed phase formation. For this purpose, solid phases, such as graphite or boron nitride, have been deliberately excluded from the species considered in the calculations. It is thus possible to account for gas "maturation", i.e. the effect of homogeneous reactions, as a function of temperature, assuming

that an infinite time is allowed for these reactions to occur. These results then describe the equilibrium of the homogeneous phase system (gas).

2.1 Calculations in the heterogeneous system

In this section, the thermodynamic equilibrium calculated for each temperature, pressure and reactive mixture includes gas and solid phases. Figure 1 shows the main gas phase species expected at equilibrium as a function of temperature and under the conditions considered, with or without ammonia. For ease of reading, only mole fractions above 10^{-8} are shown. In both cases, the main species in the gas phase at low temperatures ($T < 500$ °C) are, in decreasing order of mole fraction, are N_2, H_2, CH_4, NH_3 and HCN. N_2 and H_2 are the dominant species due to the high dilution in N_2 and the decomposition of NH_3. Their concentration is therefore only slightly affected by temperature. On the other hand, the concentration of NH_3 and CH_4 decreases with temperature, unlike HCN, C_2H_2, C_2N_2, B, H and CH_3.

Apart from the formation of a small amount of CH_3 at high temperatures, the introduction of ammonia does not appear to significantly modify the gas phase at equilibrium. It is worth noting that these calculations do not take into account the extremely high effective nitrogen and hydrogen activities of a flowing NH_3 [26]. From the thermodynamic point of view adopted here, the initial presence of NH_3 simply corresponds to a source of hydrogen and nitrogen, while the dissociation of ammonia may actually be far from complete as seen later experimentally. The exact effect of ammonia is probably not accurately described by the thermodynamic study but trends can be drawn. From about 1000 °C in the presence of NH_3, and 900 °C without NH_3, HCN becomes the third major constituent of the gas phase after H_2 and N_2. It therefore appears interesting to aim for high processing temperatures to favour the formation of HCN in order to limit the introduction of carbon into the coatings.
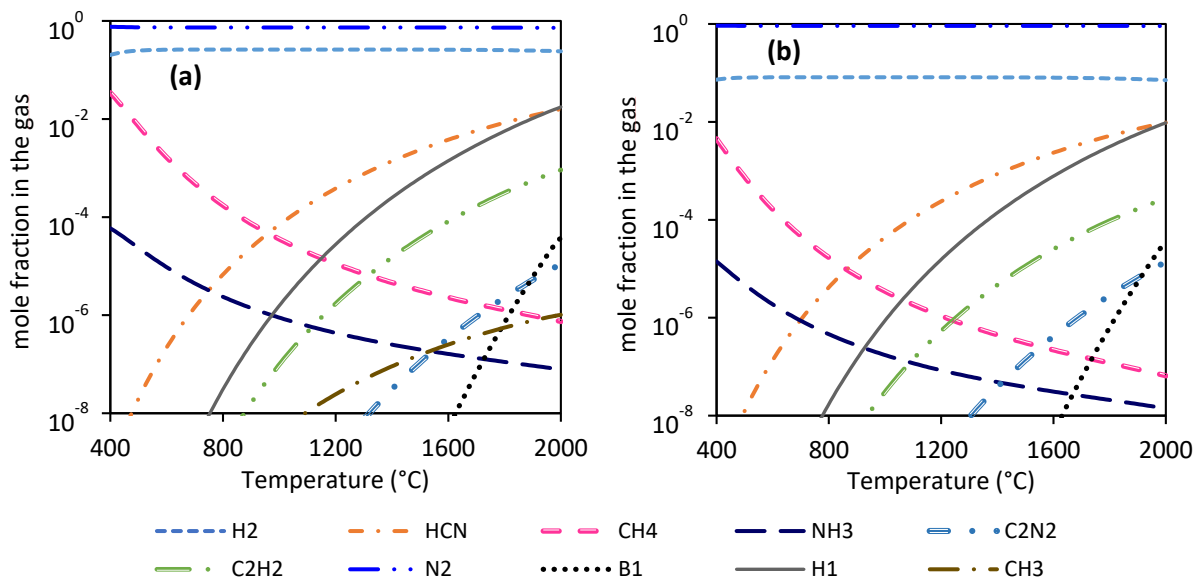

Figure 1 – Calculated mole fractions of gas phase species produced at equilibrium from TEAB/NH_3/N_2 mixture (2.5 mol TEAB, 40 mol NH_3, 212.5 mol N_2) (a) and from TEAB/N_2 mixture (2.5 mol TEAB, 252.5 mol N_2) (b) at 55 mbar as a function of temperature.

Figure 2 shows the solid phases expected under the same conditions. The solid phases mainly expected are boron nitride (BN) and graphite (C). A domain of existence of boron carbide (B$_4$C) appears at the expense of boron nitride and graphite at very high temperatures ($T > 1900$ °C) and in the presence of

ammonia. This result could be due to the slightly lower initial amount of nitrogen atoms available to form the nitride in mixture (i) than in mixture (ii), 467.2 moles versus 507.5 moles. The resulting slight excess of boron leads to the formation of the carbide.
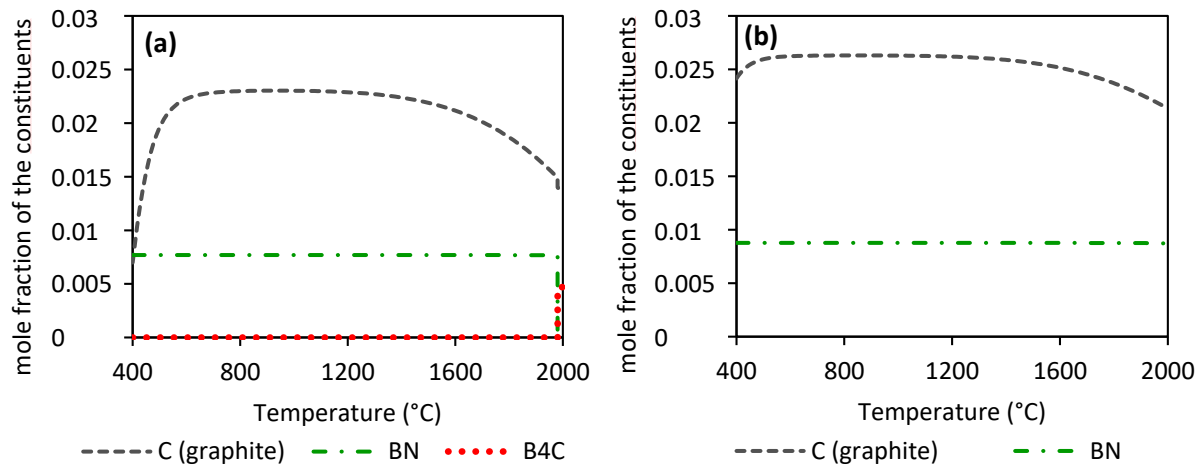

Figure 2 – Calculated mole fractions of solid species produced from TEAB/NH$_3$/N$_2$ mixture (2.5 mol TEAB, 40 mol NH$_3$, 212.5 mol N$_2$) (a) and from TEAB/N$_2$ mixture (2.5 mol TEAB, 252.5 mol N$_2$) (b) at 55 mbar as a function of temperature.

Figure 3 shows the quantities of species produced in the presence of NH$_3$ minus those produced in the absence of NH$_3$. Figure 3a and Figure 3b display the quantities of gaseous species at different scales, while Figure 3c relates to the solid phases.
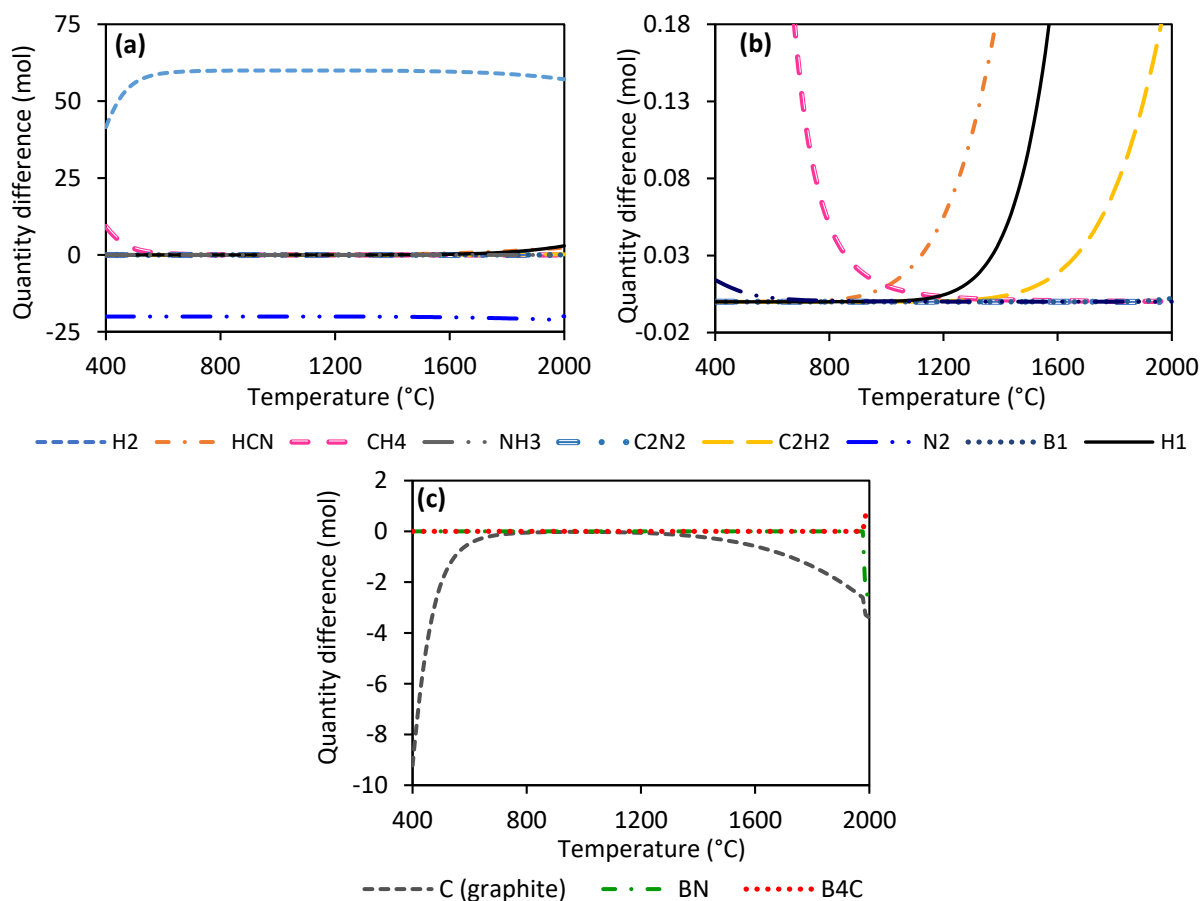
Figure 3 – Differences between the quantities of species produced from the TEAB/NH$_3$/N$_2$ mixture and those produced from the TEAB/N$_2$ mixture. Case of gaseous species (a) and (b) and case of solid species (c).

The larger initial amount of hydrogen atoms used for calculations in the system reflecting the presence of NH$_3$ favours the formation of H$_2$ over the whole temperature range, as well as CH$_4$ at low temperatures. In the intermediate range, from 900 °C to 1200 °C, the two systems behave similarly. From 1200 °C in the presence of NH$_3$, the higher hydrogen content contributes to the formation of HCN, and to the formation of C$_2$H$_2$ at higher temperature at the expense of C$_2$N$_2$. The additional source of hydrogen leads to an increase in the formation of light hydrocarbons, such as CH$_4$ below 900 °C, as well as HCN and C$_2$H$_2$ from 900 °C and 1400 °C respectively (Figure 3b). This phenomenon thus contributes to the reduction of the quantity of solid carbon (graphite) present below 800 °C and above 1300 °C (Figure 3c).

The results of calculations carried out at different pressures are presented in Figure 4. There is no effect of pressure on the quantities at equilibrium of HCN, C$_2$H$_2$ and C$_2$N$_2$. The increase in pressure results in an increase in the content of CH$_4$ and NH$_3$. The effect of pressure on the solid phases is visible at the temperature limits. An increase in pressure shifts the onset of the graphite existence to higher temperature. On the contrary, a decrease in pressure allows the appearance of B$_4$C at lower temperatures at the expense of BN. Thus, at 100 mbar, B$_4$C predominates over BN from 1840 °C. As a general rule, the effect of pressure is very limited compared to that of temperature.
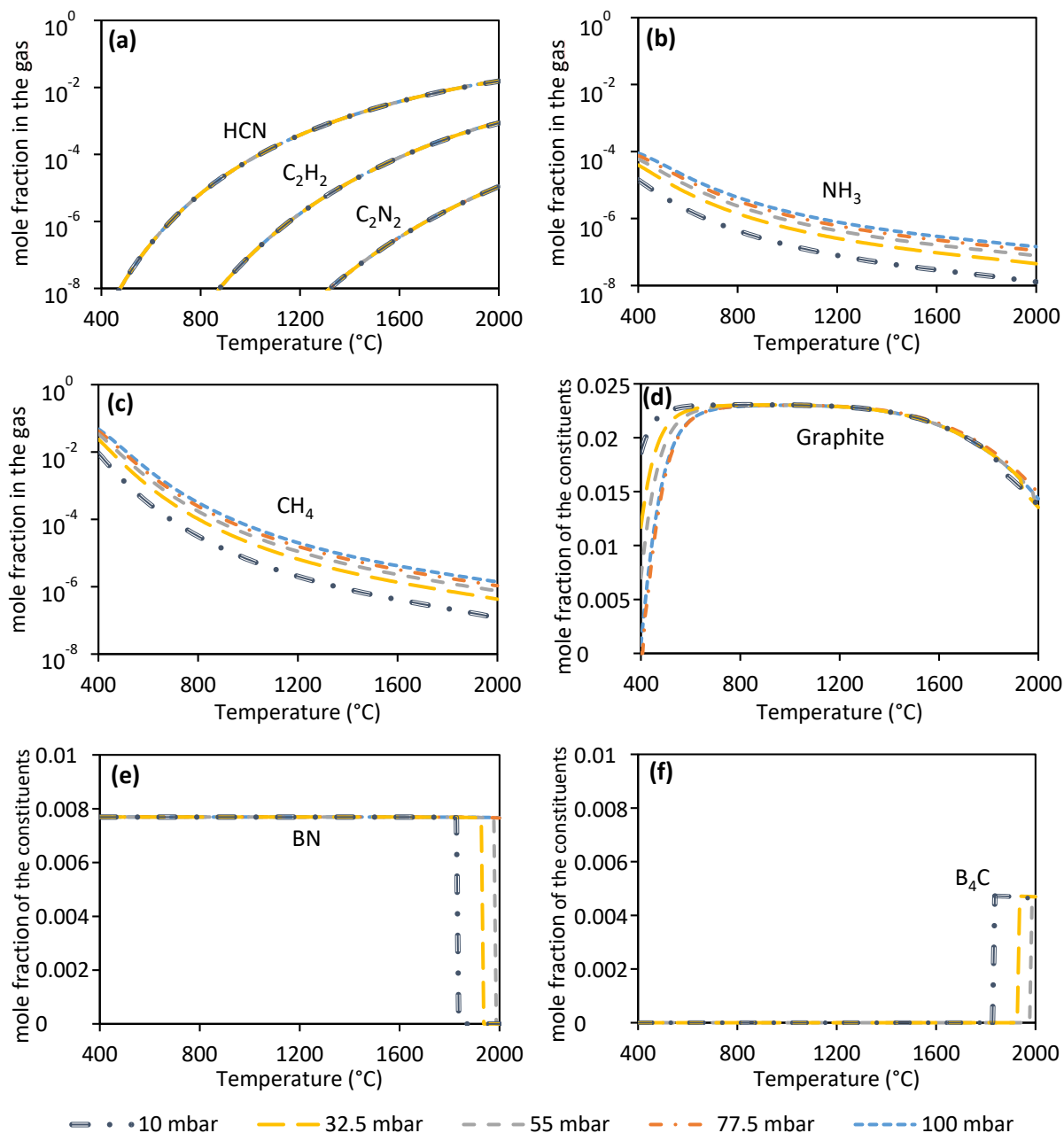
Figure 4 – Effect of pressure on the mole fraction at thermodynamic equilibrium of the main gases (a), (b) and (c) and solid phases (d), (e) and (f) produced from TEAB/NH$_3$/N$_2$ mixture (2.5 mol TEAB, 40 mol NH$_3$, 212.5 mol N$_2$)

The driving forces for the formation of each solid phase normalised by $R \cdot T$ (where R is the ideal gas constant and T the temperature) are plotted in Figure 5 in the presence and absence of NH$_3$. The driving force evolution shows no significant differences between BN and graphite over the range 800-2000 °C. For temperatures below 800 °C, BN formation seems to be the dominant reaction in both cases, but graphite formation is less favoured when ammonia is initially present. Finally, B$_4$C prevails over BN at around 2000 °C.
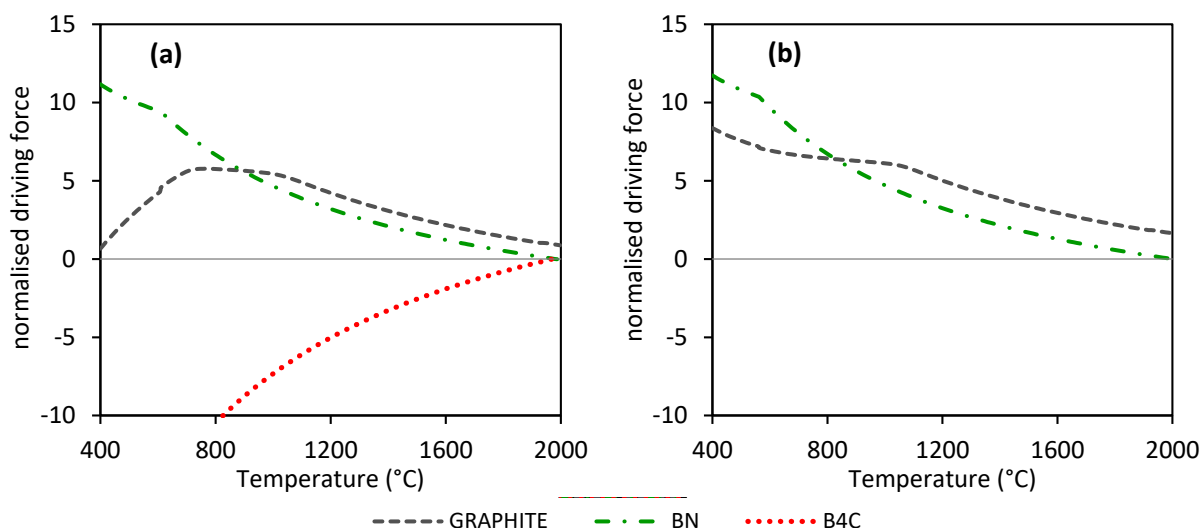
Figure 5 – Normalised driving forces for the formation of solid phases in TEAB/NH$_3$/N$_2$ mixture (2.5 mol TEAB, 40 mol NH$_3$, 212.5 mol N$_2$) (a) and in TEAB/N$_2$ mixture (2.5 mol TEAB, 252.5 mol N$_2$) (b) at 55 mbar as a function of temperature.

The addition of ammonia, i.e. essentially an additional source of hydrogen from the point of view of these calculations, will favour the formation of hydrocarbons. High temperatures enhance the formation of HCN at the expense of solid carbon. A short residence time or the use of a cold wall CVD reactor should also be more favourable to the limitation of carbon in the solid, as it limits the homogeneous phase reactions and therefore the pyrolysis of carbonaceous by-products such as C$_2$H$_2$ or CH$_4$ at high temperature, which could contaminate the deposited BN.

2.2 Calculations in the homogeneous system

In this section, the calculations relate only to gaseous species at equilibrium, solid species having been excluded from the calculations. For clarity, only the mole fractions of species greater than 10^{-6} are shown. Figure 6 shows the gas phase evolution as a function of temperature in the absence of ammonia in the initial mixture. Figure 6a shows the hydrocarbons and associated radicals, while Figure 6b shows the species containing nitrogen and/or boron.
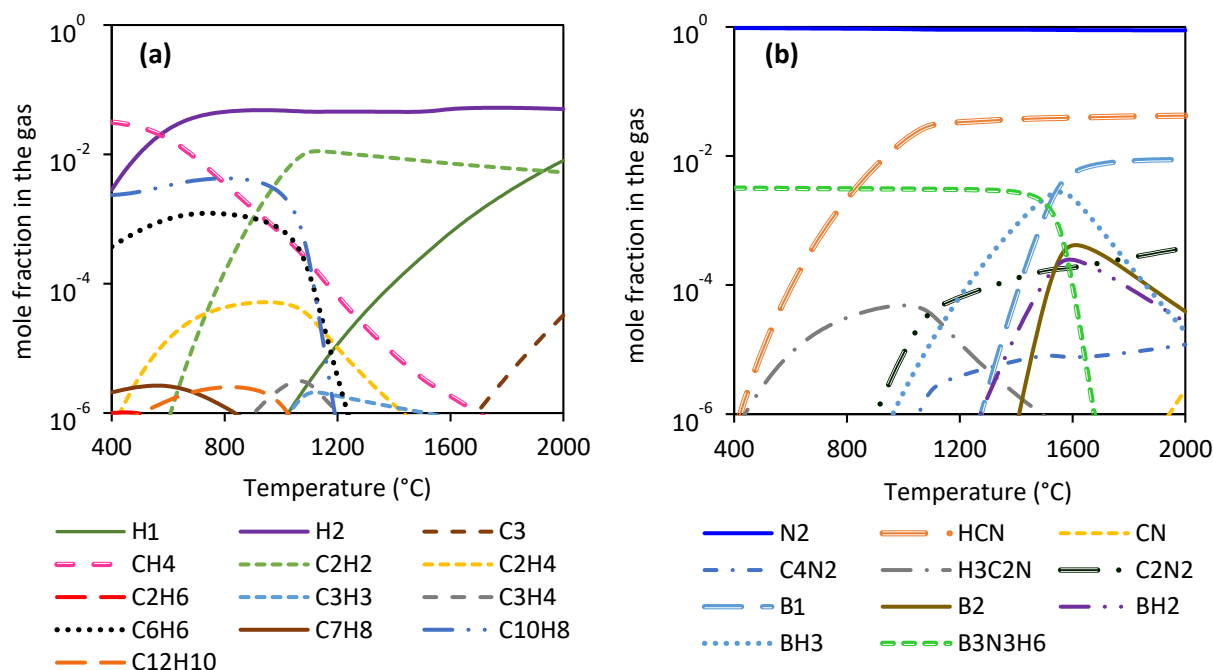
Figure 6 – Calculated mole fractions of gas phase species produced at equilibrium from TEAB/N_2 mixture (2.5 mol TEAB, 252.5 mol N_2): hydrocarbons (a), boron-containing and nitrogen-containing species (b)

In the NH_3-free system, N_2 remains the major species, followed by CH_4 below 600 °C and H_2 above. The main light hydrocarbons are CH_4 at low temperatures and by C_2H_2 at high temperatures (Figure 6a). C_2H_4 is present, in lower concentration, between 400 and 1400 °C. CH_4 decreases progressively when the temperature increases over the whole temperature range. We note the high proportion of aromatic and/or heavy hydrocarbons (C > 5) until about 1000 °C, disappearing at 1200 °C. Beyond this point, the content of these species drops in favour of HCN, C_2H_2 and H.

An existence domain of borazine appears in Figure 6b, up to 1600 °C. Beyond 1600 °C, B1 dominates the other boron-containing species and stabilises. The transition between these two domains is characterised by the presence of BH_3 and BH_2. HCN increases strongly from 400 °C and stabilises at 1100 °C, to become the third major constituent of the gas phase just after H_2. H_3C_2N appears between 400 and 1400 °C. The decrease in its mole fraction is accompanied by an increase in that of C_2N_2.

Figure 7 shows the evolution of the gas phase in the presence of NH_3. The changes caused by the presence of NH_3, i.e. by a higher amount of hydrogen in the system, are mainly noticeable for hydrocarbons at low temperatures. N_2 remains the main constituent of the gas phase in the presence of NH_3. Borazine is stable in the homogeneous system up to 1600 °C (Figure 7b), whereas it is absent in the heterogeneous system equilibrium (Figure 1). This observation indicates that borazine can be an effective precursor of BN if sufficient gas maturation is achieved without involving the borazine precursors themselves in heterogeneous reactions. The dominance of CH_4 over H_2 at low temperature disappears. H_2 thus remains the second major constituent over the whole temperature range (Figure 7a). The presence of NH_3, a source of H_2, favours the stability of CH_4 at low temperatures at the expense of aromatic and unsaturated hydrocarbons. As a result, heavy hydrocarbons appear at higher temperature but still disappear at around 1200 °C. The addition of NH_3 leads to an increase in the concentration of CH_4 and C_2H_4, as well as an extension of their respective stability domains towards high temperatures. CH_3 appears from 900 °C and stabilises at around 1200 °C on a plateau that extends to 2000 °C.
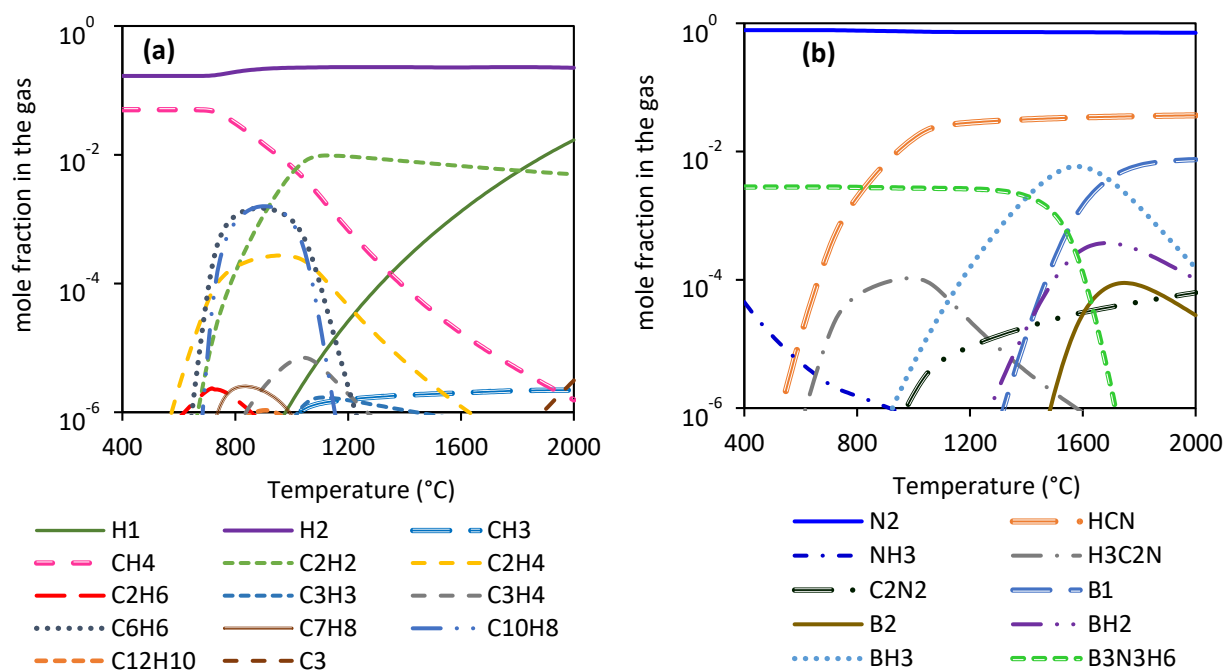
Figure 7 – Calculated mole fractions of gas phase species produced at equilibrium from TEAB/NH$_3$/N$_2$ mixture (2.5 mol TEAB, 40 mol NH$_3$, 212.5 mol N$_2$): hydrocarbons (a), boron-containing and nitrogen-containing species (b)

Only from the thermodynamic analysis, the two gas mixtures, TEAB/N$_2$ and TEAB/NH$_3$/N$_2$, give similar results. The gas phase is rich in hydrocarbons at equilibrium up to intermediate temperatures (< 1200 °C). Above this temperature, the degradation of these hydrocarbons leaves only HCN, C$_2$H$_2$ and C$_2$H$_4$ (marginally) in addition to some radicals (CH$_3$, H). The introduction of NH$_3$ is equivalent to an addition of hydrogen, which is favourable to saturated species and light hydrocarbons.

3. Experimental procedure

The CVD apparatus used was the same as that used by Carminati *et al.* [6]. It was a hot-wall reactor operating at low pressure. The temperature of the hot zone wall was measured by a type B thermocouple. The N$_2$ (purity 99.99%) and NH$_3$ (purity 99.99%) flow rates were controlled by mass flowmeters (SLA5850 from Brooks). The TEAB vapour was carried by nitrogen by bubbling in an evaporator stainless steel vessel containing liquid TEAB (97%, from Sigma Aldrich) and immersed in a thermostatic bath. To avoid contact of the TEAB with the ambient air, the evaporation vessel was filled in a glove box (GP Campus from Jacomex) under nitrogen atmosphere. The TEAB/N$_2$ gas mixture line was heated between the evaporator and the reactor to avoid condensation. For a given working pressure and carrier nitrogen flow rate, the TEAB gas flow rate was adjusted by setting the temperature of the thermostatic bath, typically at around 75 °C. The value of the TEAB gas flow rate was first calculated from its saturation vapour pressure and assuming saturation of the carrier gas. The vapour pressure of TEAB was calculated as a function of temperature using the Clausius-Clapeyron relation, the enthalpy of vaporisation value of 60.7 kJ/mol from the literature and the value of 1600 Pa for 96-97 °C given by the supplier and the literature [27,28]. The consumption of liquid TEAB measured from preliminary bubbling tests corresponded to the values expected from the calculations.

For *ex situ* gas-phase characterisation, the configuration of the Fourier-transform infrared (FTIR) spectrometer, the MCT-A detector and the room temperature gas cell connected at the reactor outlet

were the same as those used in the study of Caminati *et al.* [6] and Desenfant *et al.* [18]. The concentration of species in the analysis cell was determined from the area of the selected characteristic peaks of the absorption spectra, A_{peak}, using the Beer-Lambert law applied to gases under low pressure behaving as ideal gases [29,30]:

$$A_{\text{peak}} = \frac{\varepsilon_{\text{me}} \cdot l_{\text{cell}} \cdot P_{\text{p}}}{R \cdot T} \tag{1}$$

where ε_{me} is the molar absorption coefficient of the species over the considered wavenumber range, l_{cell} the length of the analysis cell (50 cm), P_{p} the partial pressure of the considered species in the cell and T the temperature in the cell (i.e. room temperature). The molar absorption coefficients of the hydrocarbon species were calculated from spectra from the work of Desenfant *et al.* [18], those of TEAB and NH_3 were calculated from spectra obtained with several carrier gas flow rates in this work. Reference spectra for triethylamine (TEA), diborane (B_2H_6) and HCN were obtained from the literature [31]. No molar absorption coefficient could be defined for these three species.

The main C_2H_4 peak is partly overlapped by an NH_3 peak, so the calculated C_2H_4 partial pressure may be affected. To avoid this, the C_2H_4 peak area measured in the presence of NH_3 at each temperature was subtracted from that obtained at 300 °C for NH_3 alone (no trace of C_2H_4). Thus, the offset due to NH_3 was corrected. This approximation should be taken into account when analysing the results.

The characteristic peaks and the respective molar absorption coefficients considered for each species are listed in Table 2.

species	peak position (cm^{-1})	ε_{me} (L·mol^{-1}·cm^{-1})	vibration mode	
CH_4	3085	3.2	ν	C–H
C_2H_2	730	185.4	δ	≡C–H
C_2H_4	950	142.0	γ	=C–H
NH_3	870	37.1	δ	N–H
TEAB	~2400	1307	ν	B–H
HCN	713	/	δ	≡C–H

Table 2 – Peaks and molar absorption coefficients used for FTIR analysis of gas concentrations at the reactor outlet [6,32–34] (ν: stretching, δ: in-plane bending, γ: out-of-plane bending

Transmission FTIR spectra of the gases at the reactor outlet were obtained for reactor temperatures ranging from 300 °C to 1300 °C. Three mixtures, TEAB/NH_3/N_2, TEAB/N_2 and NH_3/N_2, were studied to identify the role of NH_3 in the degradation of TEAB. The following proportions were used:

(i)   TEAB/NH_3/N_2: 2.5 sccm / 40 mol sccm / 212.5 sccm.

(ii)   TEAB/N_2: 2.5 sccm / 252.5 sccm.

(iii) NH_3/N_2: 40 sccm / 215 sccm

The total flow rate was 255 sccm and the pressure was 55 mbar, with a residence time in the hot zone of the reactor of about 0.25 s. To limit the risk of adsorption/desorption from the gas cell walls of unreacted TEAB, the measurements were started with the highest reactor temperatures (1300 °C).

Following the FTIR gas phase analysis study, a coating was deposited at 1300 °C and 55 mbar for 1h20 on a 10 mm × 10 mm silicon wafer placed in the centre of the hot zone of the CVD reactor from the TEAB/NH_3/N_2 gas mixture. Gas flow rates close to case (i) of the previous study were used, but to limit the risk of depletion in the presence of the substrate, the TEAB flow rate was increased to the

maximum possible value of 3.5 sccm. This lowered the dilution ratio of TEAB to NH_3, denoted α, from 16 to 11.

The fractured surface of the CVD coating deposited on the rough side of the wafer was observed by scanning electron microscopy (SEM, QUANTA 400 FEG) either in the secondary electrons (SE) or back-scattered electrons (BSE) detection modes with an accelerating voltage of 5 kV. Chemical analyses were also performed in the microscope by energy dispersive X-ray spectroscopy (EDS) with an Oxford Ultim® Max detector equipped with a 100 mm^2 sensor. The results were cross-checked with those obtained with a reference sample of pure boron nitride.

The sample was analysed by grazing incidence X-ray diffraction (GIXRD) using a Bruker D8 Advance ($\lambda_{CuK\alpha1}$ = 0.15419 nm). The X-ray angle of incidence was set to 1°. The pattern was acquired on a 2ϑ diffraction angle range of 22–30°, in order to focus analysis on the peak related to the diffraction from adjacent basal planes of sp^2-hybridized BN (sp^2-BN) corresponding either to (002) for hexagonal BN (2ϑ = 26.765°, JCPDS n° 00–034-0421) or to (003) for rhombohedral BN (with indexing using the hexagonal crystallographic system) [35]. d, the interreticular distance between the sp^2-BN planes, was deduced from the Bragg's law: $2d \sin(\vartheta) = n\lambda$, where n is the diffraction order taken equal to 1, λ is the wavelength of CuKα1 line and ϑ is the diffraction angle. L_c, the coherence length, was calculated from the Scherrer equation: $L_c = k\lambda / \Gamma\cos(\vartheta)$, where the constant k was taken equal to 0.89 and Γ is the full width at half maximum of the XRD peak.

4. Experimental results and discussion

4.1 FTIR gas phase analysis

Figure 8 shows the FTIR spectra obtained at the outlet of the reactor heated to 1300 °C, for the three gas mixtures. At 1300 °C, with or without the addition of NH_3, the species identified from the degradation of TEAB in the hot zone are HCN, CH_4 and C_2H_2. Their presence is consistent with thermodynamic calculations. H_2 and N_2 are assumed to be present but are not detected by FTIR. A low concentration of C_2H_4 can also be found at intermediate temperatures (spectra not shown). This species is not present at either 300 °C or 1300 °C. The appearance of ethylene at intermediate temperatures was predicted by the calculations in the homogeneous system (Figure 6a and Figure 7a). This species is thus probably involved in the deposition of carbon in the coating at 1300 °C.
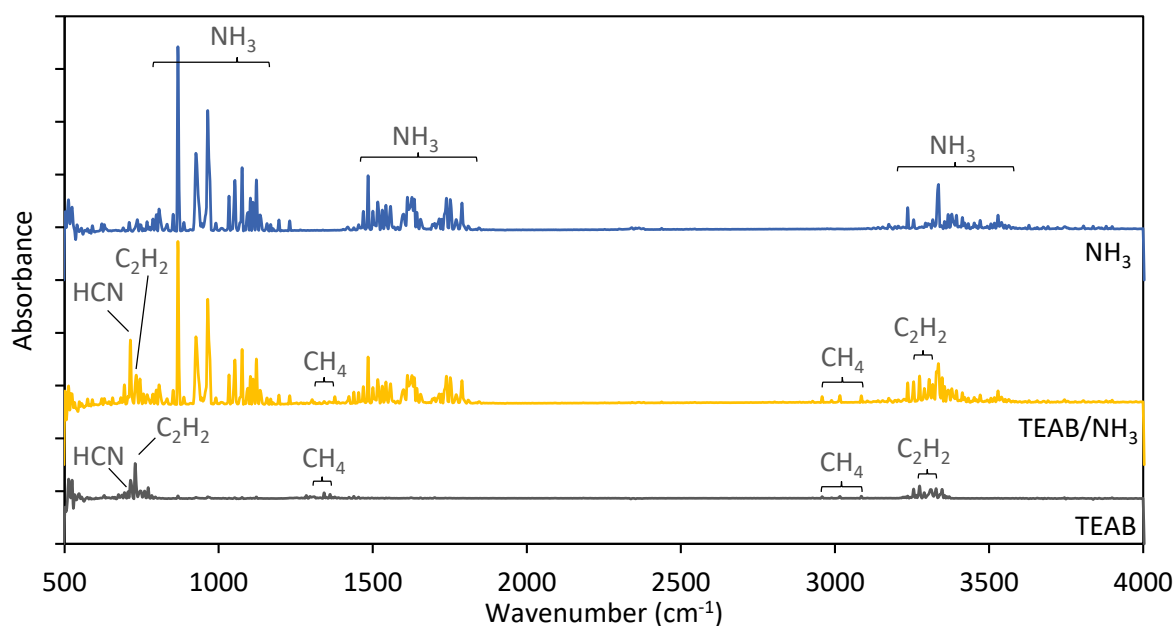
Figure 8 – FTIR spectra of the gases at the outlet of the reactor heated to 1300 °C for the different initial gas mixtures: TEAB/NH_3/N_2, TEAB/N_2 and NH_3/N_2

Figure 9a shows the FTIR spectra obtained for a reactor temperature of 300 °C. Figure 9b shows a comparison of the peaks observed between 2200 and 3200 cm^{-1} with the reference spectra of triethylamine (TEA) and diborane taken from the NIST database [31], as well as those of NH_3 and the reference TEAB obtained in this work at room temperature. TEAB was observed during the analysis of the NH_3 and N_2 mixture at 300 °C, owing to the desorption of unreacted TEAB previously absorbed on the surface of the cold parts located downstream of the hot zone. Due to the low vapour pressure of TEAB at room temperature, it was difficult to remove these traces. However, this contamination only appears at very low temperatures, i.e. in the analyses carried out last after those at high temperatures.
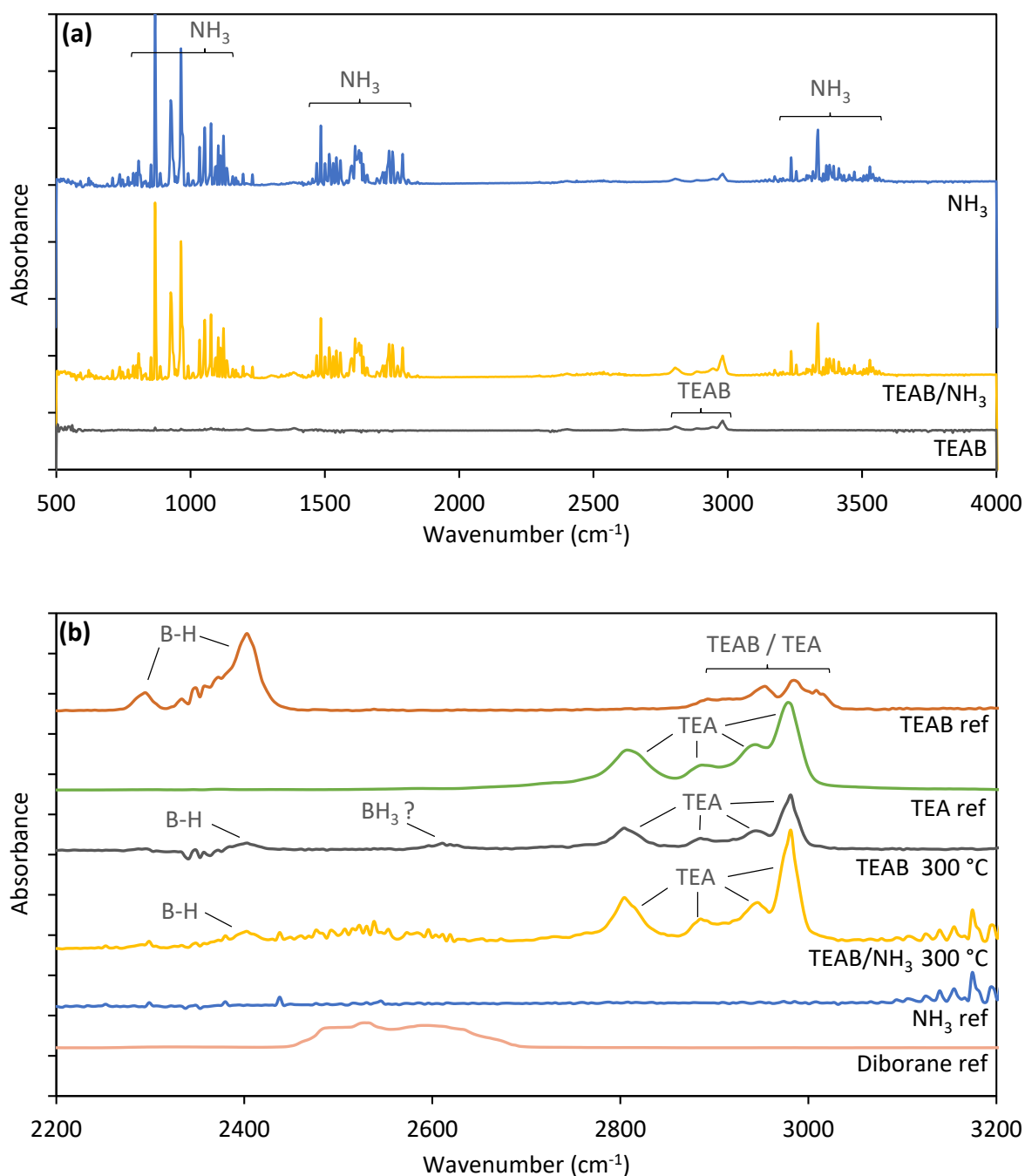
Figure 9 – FTIR spectra of the gases at the outlet of the reactor heated to 300 °C for the different initial gas mixtures: TEAB/NH₃/N₂, TEAB/N₂ and NH₃/N₂ (a) and comparison with room temperature reference spectra in the range 3200-2200 cm⁻¹ (b)

Figure 10 shows the partial pressures of each gas detected, calculated from the spectra peak areas and the molar extinction coefficients determined experimentally. As the molar absorption coefficient for HCN could not be obtained, the partial pressure of HCN is not shown in this figure. Figure 10d shows the characteristic peak area of HCN as a function of reactor temperature. The peak area is normalised by the maximum area value observed at 1300 °C. The partial pressures of TEAB are low and even more difficult to detect as part of its characteristic peaks are overlapped by those of NH₃. Therefore, the

TEAB pressure could only be calculated in the absence of NH_3. The partial pressure of C_2H_4 in the presence of NH_3 was corrected according to the method described in the experimental section.
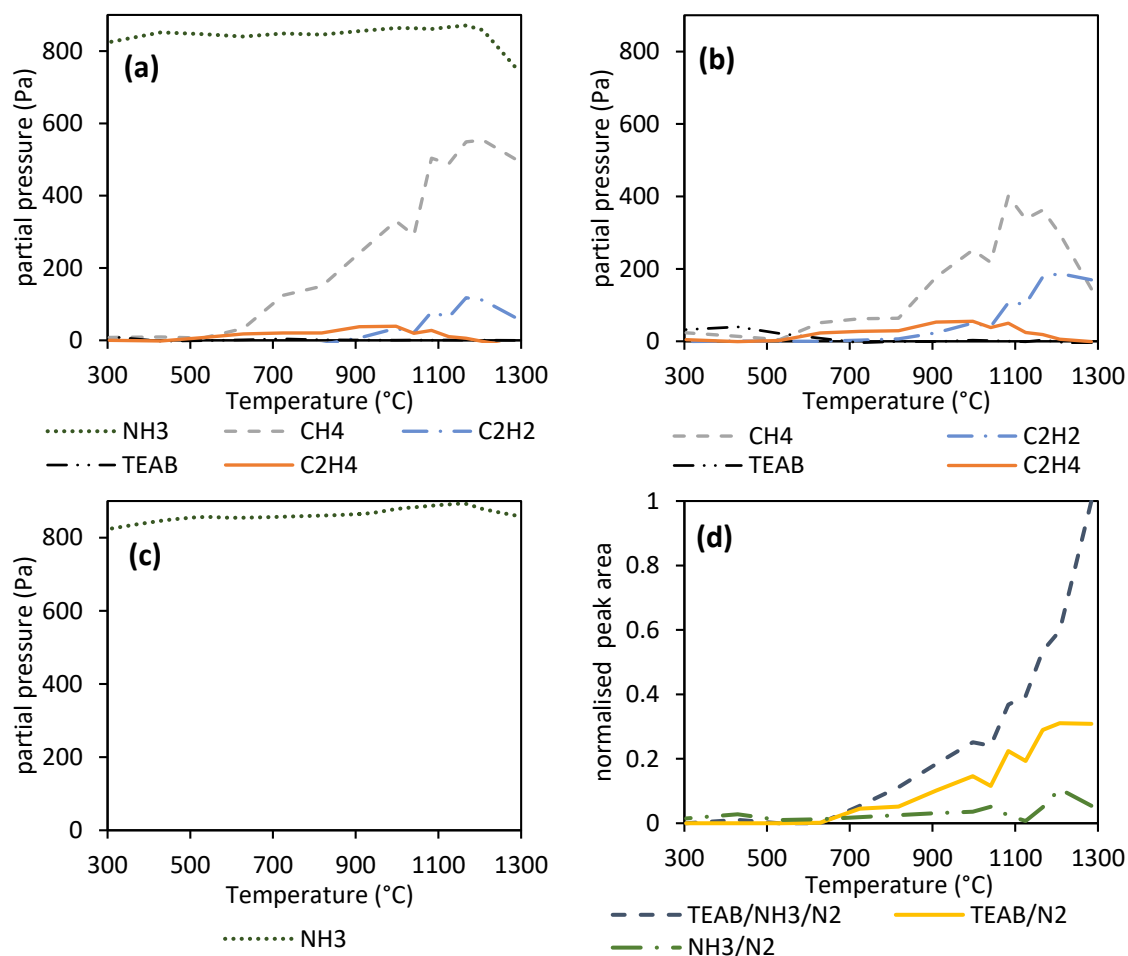

Figure 10 – Influence of temperature on the by-product partial pressures for the initial gas mixtures TEAB/NH$_3$/N$_2$ (a), TEAB/N$_2$ (b) and NH$_3$/N$_2$ (c) and on the HCN normalised peak area (d) at the reactor outlet

Although NH_3 is susceptible to decompose at high temperatures [36–38], Figure 10c shows that even with increasing temperature, the residence time in the reactor is too short to allow decomposition of NH_3 simply diluted in N_2. No other species are detected in the presence of the NH_3/N_2 mixture.

With the introduction of TEAB (Figure 10a), it is only from 1200 °C that a clear decrease in the intensity of NH_3 characteristic peak can be observed, accompanied by an increase in the HCN characteristic peaks. This behaviour suggests a consumption of ammonia in favour of the HCN formation at high temperature. The dilution of TEAB in NH_3 with α = 16 corresponds to only two moles of ammonia for one mole of carbon. However, while a strong reaction between TEAB and NH_3 was expected, the characteristic peak area of ammonia indicates that only a small fraction is degraded. This means that the system is far from thermodynamic equilibrium and that reaction and decomposition kinetics are dominant factors in the formation of the output gas mixture.

4.2 Interpretation regarding the homogeneous reactions

The peak associated with triethylamine, located at 2800 cm^{-1} [31,39], appears between 300 and 600 °C with or without NH_3. A peak associated with BH_3 and located at about 2610 cm^{-1} [40,41], visible in

Figure 9b, only appears at 300 °C in the absence of NH_3. This peak is not present in the reference spectrum of TEAB. The presence of diborane is unlikely because its main peak at 1600 cm^{-1} and the component at 2530 cm^{-1} [31] do not appear. These observations reveal the dissociation of the complex according to Eq. (2), leading to the formation of triethylamine (TEA) and borane (BH_3).

$(C_2H_5)_3N:BH_3 \rightarrow (C_2H_5)_3N + BH_3$ (2)

BH_3 is very unstable and is supposed to rapidly decompose into B_2H_6 even at low temperatures, which explains its non-detection over the rest of the temperature range. This Lewis acid also reacts with ammonia to form various aminoboranes, such as borazane (BH_3NH_3). The presence of ammonia allows the consumption of borane at 300 °C [10,14]. Conversely, in the absence of dilution in NH_3, traces of boranes are observed at the reactor outlet at this temperature.

The appearance of gaseous carbonaceous species from 500 °C implies the onset of TEA decomposition, notably into CH_4, HCN and to a lesser extent C_2H_4. Methane appears from 500 °C and its concentration increases with temperature until 1100 °C and then decreases (Figure 10b). In the presence of NH_3, the decrease in the partial pressure of CH_4 is lower in the 1100–1300 °C range (Figure 10a). Ethylene also appears at 500 °C and its partial pressure increases slightly with temperature until it reaches a maximum at 1000 °C, of about 40 Pa in the presence of NH_3 and 50 Pa in the absence of NH_3. It then decreases until it is no longer detected above 1200 °C. Acetylene appears at around 900 °C. It follows a strong growth in the 900–1200 °C range, followed by a slight decrease in the 1200–1300 °C range.

The works of Duff and Bauer [42] and of Happel and Kramer [43] on the C/H gas phase system have allowed the identification of stability temperature domains for different hydrocarbons, based on thermodynamic calculations excluding solid phases (graphite). They showed the relative stability of CH_4 at low temperature, which degrades rapidly with increasing temperature. Moreover, the existence range of C_2H_4 appears limited, with low relative concentrations from about 900 °C to 1300 °C. Finally, these works show a stability range of C_2H_2 that extends from 1200 °C to more than 2800 °C, with relative concentrations more than ten times those of C_2H_4. Figure 10a and Figure 10b are therefore in line with these previous works.

In the absence of NH_3, a strong decrease in the partial pressure of CH_4 in favour of C_2H_2 can be observed (Figure 10b) at temperatures above 1100 °C. The work of Happel and Kramer shows that the thermal decomposition of CH_4 in this temperature range leads to the formation of C_2H_2 [43] according to Eq. (3). Also, the decomposition of methane can lead to the formation of ethylene according to Eq. (4) [44,45]. Finally, C_2H_4 decomposes with temperature according to Eq. (5) [45,46], accounting for the disappearance of this gas in favour of acetylene from 1000 °C, with or without ammonia (Figure 10a and Figure 10b).

$2CH_4 \rightarrow C_2H_2 + 3H_2$ (3)

$2CH_4 \rightarrow C_2H_4 + 2H_2$ (4)

$C_2H_4 \rightarrow C_2H_2 + H_2$ (5)
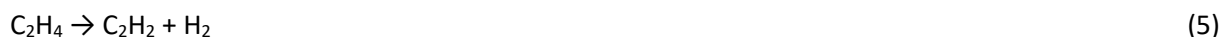
The presence of HCN is observed from 700 °C. In the presence of nitrogen radicals, resulting in particular from the amine decomposition, the formation of HCN according to Eq. (6) is envisaged, as suggested by the work of Delagrange and Schuurman [47].

$2CH_4 + 2N^* \rightarrow 2HCN + 3H_2$ (6)

From 700 °C and above, the effect of NH_3 is significant. Firstly, it promotes the formation of HCN (Figure 10d). The solid carbon possibly resulting from the decomposition of TEA reacts with NH_3 to form HCN according to Eq. (7) at temperatures above 800 °C [48–52,34].

$C + NH_3 \rightarrow HCN + H_2$ (7)

Ammonia can react with methane, as in the Degussa process, which uses a mixture of NH_3 and CH_4 with a platinum catalyst to produce HCN [53,54]. This reaction takes place from 1200 °C and above. Moreover, in the presence of CH_4 and NH_3, a reaction path proposed by Tsang *et al.* [55] introduces the intermediate species CH_3NH_2 produced from the reaction between CH_4 and the NH_2 radical, or

between NH_3 and the CH_3 radical. At high temperature ($T > 1000$ °C), the dehydrogenation of CH_3NH_2 leads to CH_2NH and then to HCN. This reaction sequence is consistent with the observations of Delagrange and Schuurman on the decomposition of CH_4 in the presence of NH_3. Indeed, a rapid decrease in CH_4 in favour of HCN has been identified under these conditions [47]. Van Dijen and Pluijmakers also detected CH_3NH_2 during the decomposition of carbon in the presence of NH_3 at temperatures above 700 °C [51]. Furthermore, this reaction sequence is commonly reported in HCN formation reactions [54,56]. The reaction between CH_4 and NH_3 is described by Eq. (8).

$$CH_4 + NH_3 \rightarrow HCN + 3H_2 \tag{8}$$

In parallel, CH_4 is formed through the reaction between carbon and NH_3 according to Eq. (9) [34]. In the presence of H_2 resulting from TEA decomposition or from HCN formation, CH_4 can also be formed through Eq. (10) [52,57].

$$C + 2NH_3 \rightarrow CH_4 + N_2 + H_2 \tag{9}$$

$$C + 2H_2 \rightarrow CH_4 \tag{10}$$

The decomposition of CH_4 is thus largely compensated, and its partial pressure at high temperatures is finally up to 3 times higher in the presence of NH_3. The partial pressure of HCN is also more than three times higher in the presence of NH_3 at 1300 °C.

The significant role of NH_3 on C_2H_2 is obvious in the range 1100–1300 °C. In this temperature range, the addition of NH_3 correlates with a decrease in C_2H_2 concentration in favour of HCN concentration. Indeed, acetylene is likely to degrade to HCN in the presence of NH_3, according to Eq. (11) [58,59].

$$C_2H_2 + 2NH_3 \rightarrow 2HCN + 3H_2 \tag{11}$$

At 1300 °C, the partial pressure of CH_4 is much higher than that of C_2H_2 as shown in Figure 10a. Conversely, the decomposition of TEAB without NH_3 in this temperature range leads to a strong rise in the partial pressure of C_2H_2 followed by a plateau of about 180 Pa (Figure 10b). The decomposition of CH_4 into C_2H_2 is slower than the formation of CH_4 produced by the pyrolysis of TEA.

The exponential growth of the HCN peak area with temperature in the presence of NH_3 and TEAB (Figure 10d) is in agreement with the thermodynamic calculations. This trend shows the high role of temperature in the formation of this gas. From 1200 °C and above, the fall in NH_3 concentration is accompanied by a sharp increase in HCN. Also, the appearance of HCN occurs at around 700 °C independently of the presence of NH_3. TEA participates in the formation of HCN. It acts as a source of nitrogen radicals for the degradation of CH_4 and allows the formation of HCN during its own decomposition. However, the area of the HCN peaks is less pronounced in the absence of NH_3, indicating a lower partial pressure and thus a lower production.

The growth of the CH_4 concentration in the 550–1200 °C range shows a different trend from the thermodynamic calculations. The residence time in this temperature range seems to be sufficiently short to limit gas maturation. The reaction kinetics are too low to allow the succession of the different expected reactions. Thus, the TEA degradation in the hot zone provides a source of CH_4 that is only partially degraded to HCN, C_2H_4, C_2H_2, or solid carbon. The CH_4 concentrations measured at the outlet of the hot zone therefore increase up to 1200 °C. Above this point, the various chemical kinetics of CH_4 decomposition become sufficiently high to compensate for its formation and lead to a fall in its concentration. The evolution of the gas phase is then consistent with the thermodynamic calculations in the range 1200–1300 °C.

The chemical reactions envisaged include the removal of carbon in the gas phase in the form of HCN and CH_4, in the presence of NH_3 and at high temperature. These conditions seem favourable for the production of pure BN coatings.

4.3 Heterogeneous reaction mechanisms

The works of Levy *et al.* [10] and Ramanuja [14] report the deposition of B-N-C-(H) coatings by LPCVD either from the TEAB/N_2 mixture between 600 °C and 850 °C, or from the TEAB/NH_3/N_2 mixture between 300 °C and 850 °C.

In the absence of NH_3 and for temperatures ranging from 650 °C to 800 °C, a chemical reaction-limited regime (CRR) is observed. The coatings deposited between 300 °C and 650 °C show a boron-rich and nitrogen-poor composition (B/C/N ≈ 55 at% / 35 at% / 10 at%). Coatings deposited at the highest temperatures contain a large carbon excess (≈ 80 at%), with nitrogen and boron as low as about 10 at%. At these high temperatures, the degradation of TEA from the dissociation of TEAB according to Eq. (2) provides the source of nitrogen and carbon, as seen previously. Borane, also produced from the dissociation of TEAB according to Eq. (2), is the source of boron.

In the presence of NH_3, the temperature at which the deposition starts is lowered to 300 °C. The atomic ratio of nitrogen to boron, measured after ion etching, increases with temperature from 0.33 at 300 °C to 0.7 at 550 °C. The carbon content is maintained at 10 at% before increasing strongly from 550 °C, to reach about 80 at% at 850 °C. The growth kinetics show a first CRR in the 250–400 °C range. The authors then observe a decrease in the growth rate between 400 and 700 °C, followed by a further increase in the growth rate, suggesting a second CRR in the 700–850 °C range.

From 600 °C and above, whether in the absence or presence of NH_3, the authors found similar chemical compositions of the coatings, which vary similarly with increasing temperature. This suggests an identical BNC deposition mechanism for both TEAB/N_2 and TEAB/NH_3/N_2 mixtures for $T > 600$ °C.

In the case of a TEAB/NH_3/N_2 mixture, the nitrogen is supplied from ammonia for temperatures below the degradation of the amine ($T < 550$ °C). The reaction for the formation of BN from borane and NH_3 corresponds to Eq. (12). The excess boron and the low carbon content in the coatings deposited at low temperatures suggest a co-deposition of boron and BN.

$$2BH_3 + 2NH_3 \rightarrow 2BN_{(s)} + 3H_2 \tag{12}$$

With increasing temperature, the BN formation reaction becomes dominant. The low carbon content and the boron/nitrogen ratio measured by the authors after ionic etching, close to 0.7 at 550 °C, suggest the presence of stoichiometric BN with low carbon contamination, taking into account the preferential etching of N over B as reported in Refs. [7,60]. The decrease in growth rate in the 400–700 °C range is related to the gaseous depletion of borane and the fact that TEA does not contribute to the coating deposition process.

As can be observed in Figure 10a, the partial pressure of CH_4 (500 Pa) is about 8 times higher than that of C_2H_2 (60 Pa) at 1300 °C, and about 9 times higher than that of TEAB introduced at the reactor inlet (54 Pa). The amount of carbon evacuated in the gas in this case is greater than that produced from TEAB alone. This inconsistency may be due to the reaction of the carbon walls of the reactor, or the carbon heat shields, with the gas mixture at such temperatures.

From the literature and the gas products identified in the present work, the decomposition of TEAB in the presence of ammonia can be described according to the general balance equation Eq. (13). Table 3 summarises the main reaction mechanisms identified for the different temperature ranges.

$$(C_2H_5)_3N{:}BH_3 + NH_3 \rightarrow BN_{(s)} + aC_{(s)} + HCN_{(g)} + bCH_{4(g)} + cC_2H_{2(g)} + dC_2H_{4(g)} + eH_{2(g)} \tag{13}$$
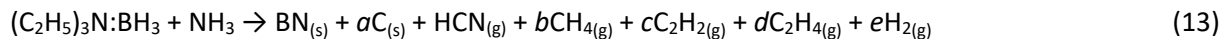
with $a + b + 2c + 2d = 5$ and $2b + c + 2d + e = 10$.

range	reaction mechanism
$T > 250\ ^\circ$C	dissociation of TEAB; reaction between BH_3 and NH_3
$T > 500\ ^\circ$C	degradation of TEA; formation of HCN, CH_4 and C_2H_4
$T > 900\ ^\circ$C	formation of C_2H_2
$T > 1200\ ^\circ$C	degradation of C_2H_4

Table 3 – Reaction mechanisms involved in the decomposition of TEAB in the presence of NH_3 for the different temperature ranges

NH_3 plays a dual role, as a source of hydrogen and as a reagent for HCN formation. The addition of NH_3 to the TEAB/N_2 mixture therefore promotes the formation of HCN and CH_4, which allow the carbon initially present in the BN precursor to be removed in the gas phase. It is thus an efficient way of limiting the carbon contamination of coatings deposited from TEAB. High temperatures (> 900 °C) are favourable for the removal of carbon in the form of HCN, but also of light hydrocarbons. The chosen dilution ratio of TEAB in ammonia (α = 16) appears to be more than sufficient, for the chosen residence time (0.25 s), in the temperature range 300–1300 °C, since more than 90% of the initial NH_3 comes out unreacted of the hot zone. The dilution chosen for the subsequent deposition experiment, α = 11, should then be high enough to prevent contamination of the BN coating by carbon.

4.4 CVD coating deposition

Figure 11 shows the fracture surface morphology of the deposit. It covers the entire surface of the Si wafer and does not show any crack or porosity at this magnification. The thin layer has a uniform thickness of 1.7 μm over the observed surface and appears slightly rough.
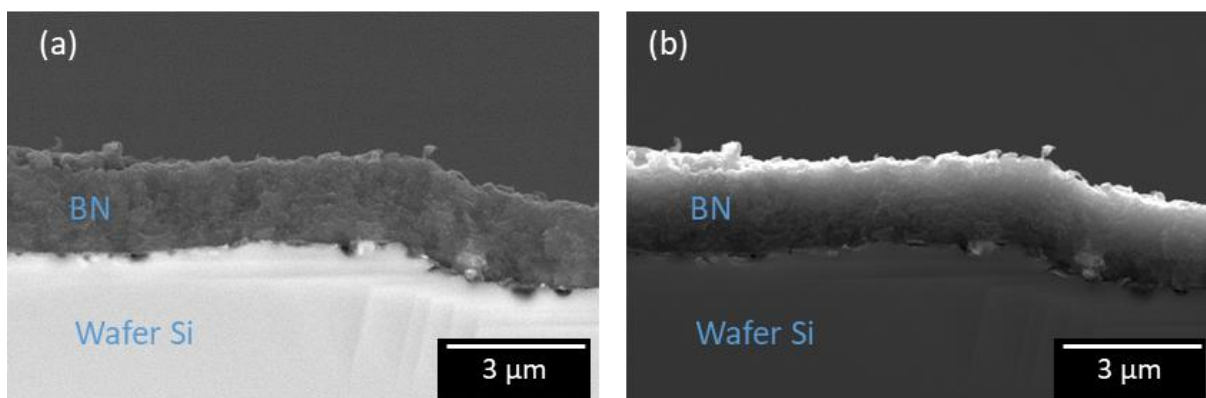

Figure 11 – SEM observation of the BN coating in BSE (a) and SE detection mode (b)

EDS analysis shows the presence of 47 at% boron and 46 at% nitrogen. The other elements detected correspond to approximately 5 at% carbon and 1 at% oxygen. These values, corresponding to the detection limits of oxygen and carbon for this preparation and analysis method, are therefore negligible. The coating consists of a stoichiometric mixture of boron and nitrogen, without significant carbon. Under these conditions, Eq. (13) can be written with a = 0.

The GIXRD pattern of the coating shows a broad peak at 25.8° related to the basal planes of sp^2-hybridised BN (Figure 12). This peak position is shifted towards smaller angles compared to the

theoretical value of 26.8° expected for hexagonal BN or for rhombohedral BN. Such a shift is classical for turbostratic BN [61,62]. This particular feature arises from the presence of a partially organised structure with many defects inducing a deformation of the crystal lattice. The interreticular distance d is 0.342 nm, higher than the theoretical value of $d_{002} = 0.333$ nm for hexagonal BN [6,63]. The calculated crystallite size L_c is 4 nm. These crystal parameters suggest close similarities with the BN coatings obtained between 1000 and 1100 °C by Carminati *et al.* by CVD from a BCl_3/NH_3 gas mixture [6]. It is worth noting the presence of a shoulder in the diffraction peak in Figure 12, at around 26.6° ($d = 0.335$ nm), suggesting a minor contribution from better crystallised domains with fewer defects. Such an asymmetry of the basal plane diffraction peak is often found in the literature on hot wall CVD coatings of BN ex-BCl_3/NH_3 [6,64,65]. It is also associated with the coexistence of two distinct BN microstructures.

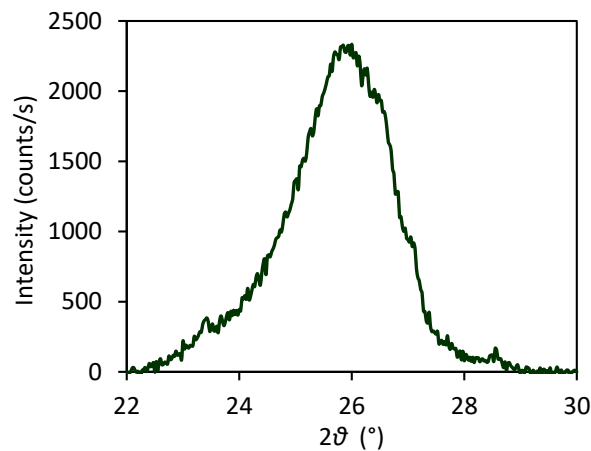These results are therefore representative of a weakly crystallised turbostratic boron nitride.

Figure 12 – GIXRD pattern of the coating deposited by CVD

5. Conclusion

The thermodynamic study showed the feasibility of producing BN from TEAB. Several ranges of experimental conditions favourable to the limitation of solid carbon were identified. Thus, the use of high deposition temperatures is favourable to the formation of gaseous carbon species. Moreover, the addition of NH_3, acting as a source of H_2, accentuates this trend.

The gas analysis of the exit of the hot zone of a hot-wall CVD reactor has identified different decomposition modes of TEAB. The formation of gaseous carbonaceous species, such as HCN, CH_4 and C_2H_2, is maximal for temperatures above 900 °C and with the addition of NH_3. It therefore appears essential to run the CVD experiments at high temperatures to evacuate carbon, mainly in the form of HCN and CH_4. The species detected by FTIR spectroscopy are consistent with thermodynamic predictions, although kinetic effects play an important role in the process. The formation of solid carbon is thus limited for short residence times. The use of a cold wall reactor would therefore seem ideal to limit the amount of co-deposited solid carbon.

Finally, a homogeneous BN coating was synthesised by isothermal CVD on a Si wafer at 1300 °C and 55 mbar. The crystal structure of this coating, characterised by XRD, appears to be similar to that of turbostratic BN made from the BCl_3/NH_3 mixture. Hence, the $TEAB/NH_3/N_2$ mixture appears to be an attractive non-chlorine alternative precursor system for the deposition of BN films by CVD.

Acknowledgements

References

[1] J. Eichler, C. Lesniak, Boron nitride (BN) and BN composites for high-temperature applications, J. Eur. Ceram. Soc. 28 (2008) 1105–1109. https://doi.org/10.1016/j.jeurceramsoc.2007.09.005.

[2] R.R. Naslain, The design of the fibre-matrix interfacial zone in ceramic matrix composites, Composites Part A: Applied Science and Manufacturing. 29 (1998) 1145–1155. https://doi.org/10.1016/S1359-835X(97)00128-0.

[3] M. Chen, L. Pan, X. Xia, W. Zhou, Y. Li, Boron nitride (BN) and BN based multiple-layer interphase for SiC$_f$/SiC composites: A review, Ceram. Int. (2022) S0272884222024087. https://doi.org/10.1016/j.ceramint.2022.07.021.

[4] P. Fenetaud, S. Jacques, SiC/SiC ceramic matrix composites and BN interphase developed for aircraft engines, Open Ceramics. Submitted (2023).

[5] G.S. Corman, K.L. Luthra, Melt infiltrated ceramic composites (Hipercomp) for gas turbine engine applications, 2006. https://doi.org/10.2172/936318.

[6] P. Carminati, T. Buffeteau, N. Daugey, G. Chollon, F. Rebillat, S. Jacques, Low pressure chemical vapour deposition of BN: relationship between gas phase chemistry and coating microstructure, Thin Solid Films. 664 (2018) 106–114. https://doi.org/10.1016/j.tsf.2018.08.020.

[7] S. Jacques, B. Bonnetot, M.-P. Berthet, H. Vincent, BN interphase processed by LP-CVD from tris(dimethylamino)borane and characterized using SiC/SiC minicomposites, in: E. Lara-Curzio, M.J. Readey (Eds.), Ceramic Engineering and Science Proceedings, John Wiley & Sons, Inc., Hoboken, NJ, USA, 2004: pp. 123–128. https://doi.org/10.1002/9780470291191.ch20.

[8] C. Lorrette, P. Weisbecker, S. Jacques, R. Pailler, J.M. Goyhénèche, Deposition and characterization of hex-BN coating on carbon fibres using tris(dimethylamino)borane precursor, J. Eur. Ceram. Soc. 27 (2007) 2737–2743. https://doi.org/10.1016/j.jeurceramsoc.2006.10.010.

[9] J.M. Grow, R.A. Levy, Micromechanical characterization of chemically vapor deposited ceramic films, J. Mater. Res. 9 (1994) 2072–2078. https://doi.org/10.1557/JMR.1994.2072.

[10] R.A. Levy, E. Mastromatteo, J.M. Grow, V. Paturi, W.P. Kuo, H.J. Boeglin, R. Shalvoy, Low pressure chemical vapor deposition of B-N-C-H films from triethylamine borane complex, J. Mater. Res. 10 (1995) 320–327. https://doi.org/10.1557/JMR.1995.0320.

[11] T. Thamm, K.-U. Körner, W. Bohne, E. Strub, J. Röhrich, S. Stöckel, G. Marx, Characterization of PECVD boron carbonitride layers, Appl. Surf. Sci. 252 (2005) 223–226. https://doi.org/10.1016/j.apsusc.2005.02.041.

[12] P.S. Hoffmann, O. Baake, M.L. Kosinova, B. Beckhoff, A. Klein, B. Pollakowski, V.A. Trunova, V.S. Sulyaeva, F.A. Kuznetsov, W. Ensinger, Chemical bonds and elemental compositions of BC$_x$N$_y$ layers produced by chemical vapor deposition with trimethylamine borane, triethylamine borane, or trimethylborazine: Chemical identification by XPS and TXRF-NEXAFS, X-Ray Spectrom. 41 (2012) 240–246. https://doi.org/10.1002/xrs.2387.

[13] O. Baake, P.S. Hoffmann, M.L. Kosinova, A. Klein, B. Pollakowski, B. Beckhoff, N.I. Fainer, V.A. Trunova, W. Ensinger, Analytical characterization of BC$_x$N$_y$ films generated by LPCVD with triethylamine borane, Anal. Bioanal. Chem. 398 (2010) 1077–1084. https://doi.org/10.1007/s00216-010-3965-4.

[14] N. Ramanuja, Low pressure chemical vapor deposition of boron nitride thin films from triethylamine borane complex and ammonia, Theses, New Jersey Institute of Technology, 1998. https://digitalcommons.njit.edu/theses/954/.

[15] M.L. Kosinova, N.I. Fainer, Yu.M. Rumyantsev, A.N. Golubenko, F.A. Kuznetsov, LPCVD boron carbonitride films from triethylamine borane, J. Phys. IV France. 09 (1999) Pr8-915-Pr8-921. https://doi.org/10.1051/jp4:19998115.

[16] C. Rohr, J.-H. Boo, W. Ho, The growth of hexagonal boron nitride thin films on silicon using single source precursor, Thin Solid Films. 322 (1998) 9–13. https://doi.org/10.1016/S0040-6090(97)01007-9.

[17] I.S. Merenkov, I.A. Kasatkin, E.A. Maksimovskii, N.I. Alferova, M.L. Kosinova, Vertically aligned layers of hexagonal boron nitride: PECVD synthesis from triethylaminoborane and structural features, J. Struct. Chem. 58 (2017) 1018–1024. https://doi.org/10.1134/S0022476617050237.

[18] A. Desenfant, G. Laduye, G.L. Vignoles, G. Chollon, Kinetic and gas-phase study of the chemical vapor deposition of silicon carbide from $C_2H_3SiCl_3/H_2$, J. Ind. Eng. Chem. 94 (2021) 145–158. https://doi.org/10.1016/j.jiec.2020.10.029.

[19] N. Saunders, A.P. Miodownik, CALPHAD calculation of phase diagrams: a comprehensive guide, Transferred to digital print, Pergamon, Oxford, 2005.

[20] H.L. Lukas, S.G. Fries, B. Sundman, Computational thermodynamics: the calphad method, Cambridge Univ. Press, Cambridge, 2007.

[21] J.-O. Andersson, T. Helander, L. Höglund, P. Shi, B. Sundman, Thermo-Calc & DICTRA, computational tools for materials science, Calphad. 26 (2002) 273–312. https://doi.org/10.1016/S0364-5916(02)00037-8.

[22] A.T. Dinsdale, SGTE data for pure elements, Calphad. 15 (1991) 317–425. https://doi.org/10.1016/0364-5916(91)90030-N.

[23] H. Duschanek, P. Rogl, H.L. Lukas, A critical assessment and thermodynamic calculation of the boron-carbon-titanium (B-C-Ti) ternary system, JPE. 16 (1995) 46–60. https://doi.org/10.1007/BF02646248.

[24] M.D. Allendorf, C.F. Melius, Thermochemistry of molecules in the B−N−Cl−H system: *ab initio* predictions using the BAC-MP4 method, J. Phys. Chem. A. 101 (1997) 2670–2680. https://doi.org/10.1021/jp962905y.

[25] B.J. McBride, M.J. Zehe, S. Gordon, NASA Glenn coefficients for calculating thermodynamic properties of individual species, Glenn Research Center, Cleveland, Ohio, 2002. https://ntrs.nasa.gov/citations/20020085330.

[26] M. Katsura, Thermodynamics of nitride and hydride formation by the reaction of metals with flowing NH_3, J. Alloys Compd. 182 (1992) 91–102. https://doi.org/10.1016/0925-8388(92)90578-W.

[27] N.K. Smith, W.D. Good, Enthalpy of formation of triethylamineborane, J. Chem. Eng. Data. 12 (1967) 570–572. https://doi.org/10.1021/je60035a026.

[28] H.L. Finke, S.S. Todd, J.F. Messerly, Trimethylamineborane and triethylamineborane: low-temperature thermodynamic properties, J. Chem. Thermodyn. 2 (1970) 129–138. https://doi.org/10.1016/0021-9614(70)90072-8.

[29] A. Beer, Bestimmung der Absorption des rothen Lichts in farbigen Flüssigkeiten, Ann. Phys. Chem. 162 (1852) 78–88. https://doi.org/10.1002/andp.18521620505.

[30] D.F. Swinehart, The Beer-Lambert law, J. Chem. Educ. 39 (1962) 333. https://doi.org/10.1021/ed039p333.

[31] P. Linstrom, NIST Chemistry WebBook, NIST Standard Reference Database 69, (1997). https://doi.org/10.18434/T4D303.

[32] O. Féron, F. Langlais, R. Naslain, Analysis of the gas phase by in situ FTIR spectrometry and mass spectrometry during the CVD of pyrocarbon from propane, Chem. Vap. Deposition. 5 (1999) 37–47. https://doi.org/10.1002/(SICI)1521-3862(199901)5:1<37::AID-CVDE37>3.0.CO;2-8.

[33] A.W. Mugenda, O. Busari, A. Benhidjeb-Carayon, T.L. Pourpoint, FTIR analysis of triethylamine borane and white fuming nitric acid gaseous combustion products, in: 51st AIAA/SAE/ASEE Joint

Propulsion Conference, American Institute of Aeronautics and Astronautics, Orlando, FL, 2015. https://doi.org/10.2514/6.2015-3755.

[34] G. Chollon, The high temperature reaction of ammonia with carbon and SiC–C ceramics, J. Eur. Ceram. Soc. 41 (2021) 136–147. https://doi.org/10.1016/j.jeurceramsoc.2020.08.066.

[35] M. Chubarov, H. Högberg, A. Henry, H. Pedersen, Review Article: Challenge in determining the crystal structure of epitaxial 0001 oriented sp^2 -BN films, Journal of Vacuum Science & Technology A: Vacuum, Surfaces, and Films. 36 (2018) 030801. https://doi.org/10.1116/1.5024314.

[36] T.V. Choudhary, C. Sivadinarayana, D.W. Goodman, Catalytic ammonia decomposition: COx-free hydrogen production for fuel cell applications, Catal. Lett. 72 (2001) 197–201. https://doi.org/10.1023/A:1009023825549.

[37] K. Kiełbasa, R. Pelka, W. Arabczyk, Studies of the kinetics of ammonia decomposition on promoted nanocrystalline iron using gas phases of different nitriding degree, J. Phys. Chem. A. 114 (2010) 4531–4534. https://doi.org/10.1021/jp9099286.

[38] F. Schüth, R. Palkovits, R. Schlögl, D.S. Su, Ammonia as a possible element in an energy infrastructure: catalysts for ammonia decomposition, Energy Environ. Sci. 5 (2012) 6278–6289. https://doi.org/10.1039/C2EE02865D.

[39] N.S. Nhlapo, W.W. Focke, E. Vuorinen, TGA–FTIR study of the vapors released by triethylamine–acetic acid mixtures, Thermochim. Acta. 546 (2012) 113–119. https://doi.org/10.1016/j.tca.2012.07.029.

[40] K. Kawaguchi, Fourier transform infrared spectroscopy of the BH_3 v_3 band, J. Chem. Phys. 96 (1992) 3411–3415. https://doi.org/10.1063/1.461942.

[41] C.W. Bauschlicher, A. Ricca, On the interaction of CO and NH_3 with BH_3 and BF_3, Chem. Phys. Lett. 237 (1995) 14–19. https://doi.org/10.1016/0009-2614(95)00269-A.

[42] R.E. Duff, S.H. Bauer, Equilibrium composition of the C/H system at elevated temperatures, J. Chem. Phys. 36 (1962) 1754–1767. https://doi.org/10.1063/1.1701262.

[43] J. Happel, L. Kramer, Acetylene and hydrogen from the pyrolysis of methane, Ind. Eng. Chem. 59 (1967) 39–50. https://doi.org/10.1021/ie50685a008.

[44] R.C. Cantelo, The thermal decomposition of methane, J. Phys. Chem. 28 (1924) 1036–1048. https://doi.org/10.1021/j150244a003.

[45] W.C. Gardiner, ed., Gas-Phase Combustion Chemistry, Springer New York, New York, NY, 2000. https://doi.org/10.1007/978-1-4612-1310-9.

[46] T. Tanzawa, W.C. Gardiner, Thermal decomposition of ethylene, Combust. Flame. 39 (1980) 241–253. https://doi.org/10.1016/0010-2180(80)90021-8.

[47] S. Delagrange, Y. Schuurman, HCN synthesis from methane and ammonia over platinum, Catal. Today. 121 (2007) 204–209. https://doi.org/10.1016/j.cattod.2006.05.089.

[48] R.M. Badger, The ammonia, carbon, hydrogen cyanide, hydrogen equilibrium and the free energy of hydrogen cyanide, J. Am. Chem. Soc. 46 (1924) 2166–2172. https://doi.org/10.1021/ja01675a003.

[49] T.K. Sherwood, E.R. Gilliland, S.W. Ing, Hydrogen cyanide synthesis from elements and from ammonia and carbon, Ind. Eng. Chem. 52 (1960) 601–604. https://doi.org/10.1021/ie50607a030.

[50] T.K. Sherwood, R.O. Maak, The reaction of ammonia with carbon at elevated temperatures, Ind. Eng. Chem. Fund. 1 (1962) 111–115. https://doi.org/10.1021/i160002a008.

[51] F.K. van Dijen, J. Pluijmakers, The removal of carbon or carbon residues from ceramic powders or greenware with ammonia, J. Eur. Ceram. Soc. 5 (1989) 385–390. https://doi.org/10.1016/0955-2219(89)90043-5.

[52] P. Dibandjo, L. Bois, F. Chassagneux, J.M. Letoffe, P. Miele, Influence of the thermal process of carbon template removal in the mesoporous boron nitride synthesis, J. Porous Mater. 15 (2008) 13–20. https://doi.org/10.1007/s10934-006-9046-6.

[53] F. Endter, Die technische synthese von cyanwasserstoff aus methan und ammoniak ohne zusatz von sauerstoff, Chemie Ing. Techn. 30 (1958) 305–310. https://doi.org/10.1002/cite.330300506.

[54] J. Gómez-Díaz, N. López, Mechanistic switch between oxidative (Andrussow) and nonoxidative (Degussa) formation of HCN on Pt(111) by density functional theory, J. Phys. Chem. C. 115 (2011) 5667–5674. https://doi.org/10.1021/jp1093349.

[55] R.S. Tsang, C.A. Rego, P.W. May, M.N.R. Ashfold, K.N. Rosser, Examination of the effects of nitrogen on the CVD diamond growth mechanism using in situ molecular beam mass spectrometry, Diam. Relat. Mater. 6 (1997) 247–254. https://doi.org/10.1016/S0925-9635(96)00647-4.

[56] L. Andrussow, Über die katalytische oxydation von ammoniak-methan-gemischen zu blausäure, Angew. Chem. 48 (1935) 593–595. https://doi.org/10.1002/ange.19350483702.

[57] K. Hedden, Die methanbildung aus wasserstoff und kohlenstoff bei hohen temperaturen und drucken, Z. Elektrochem., Ber. Bunsenges. Phys. Chem. 66 (1962) 652–661.

[58] J.P. Ferris, Yoji. Ishikawa, Formation of hydrogen cyanide and acetylene oligomers by photolysis of ammonia in the presence of acetylene: applications to the atmospheric chemistry of Jupiter, J. Am. Chem. Soc. 110 (1988) 4306–4312. https://doi.org/10.1021/ja00221a033.

[59] E. Vyazmina, J. Sheng, S. Jallais, L. Bustamante-Valencia, P. Bruchet, F.P. Richard, Carbonitriding: kinetic modeling of ammonia and acetylene decomposition at high temperature and low pressure, Mater. Tech. 106 (2018) 103. https://doi.org/10.1051/mattech/2018033.

[60] C. Guimon, D. Gonbeau, G. Pfister-Guillouzo, O. Dugne, A. Guette, R. Naslain, M. Lahaye, XPS study of BN thin films deposited by CVD on SiC plane substrates, Surf. Interface Anal. 16 (1990) 440–445. https://doi.org/10.1002/sia.740160191.

[61] S. Le Gallet, G. Chollon, F. Rebillat, A. Guette, X. Bourrat, R. Naslain, M. Couzi, J.L. Bruneel, Microstructural and microtextural investigations of boron nitride deposited from BCl_3–NH_3–H_2 gas mixtures, J. Eur. Ceram. Soc. 24 (2004) 33–44. https://doi.org/10.1016/S0955-2219(03)00126-2.

[62] N. Coudurier, M. Chubarov, R. Boichot, F. Mercier, E. Blanquet, R. Reboud, S. Lay, A. Crisci, S. Coindeau, T. Encinas, M. Pons, Growth of boron nitride films on w-AlN (0001), 4° off-cut 4H-SiC (0001), W (110) and Cr (110) substrates by Chemical Vapor Deposition, Cryst. Res. Technol. 51 (2016) 231–238. https://doi.org/10.1002/crat.201500284.

[63] Y. Shi, C. Hamsen, X. Jia, K.K. Kim, A. Reina, M. Hofmann, A.L. Hsu, K. Zhang, H. Li, Z.-Y. Juang, Mildred.S. Dresselhaus, L.-J. Li, J. Kong, Synthesis of few-layer hexagonal boron nitride thin film by chemical vapor deposition, Nano Lett. 10 (2010) 4134–4139. https://doi.org/10.1021/nl1023707.

[64] H. Plaisantin, S. Jacques, J. Danet, G. Camus, H. Delpouve, TEM characterization of turbostratic and rhombohedral BN interphases synthesized by chemical vapour infiltration in SiC/SiC-Si composites, Mater. Charact. 172 (2021) 110857. https://doi.org/10.1016/j.matchar.2020.110857.

[65] T. Takahashi, H. Itoh, A. Takeuchi, Chemical vapor deposition of hexagonal boron nitride thick film on iron, J. Cryst. Growth. 47 (1979) 245–250. https://doi.org/10.1016/0022-0248(79)90248-3.